JOURNAL OF GEOPHYSICAL RESEARCH, VOL. 106, NO. E11, PAGES 27,825–27,839, NOVEMBER 25, 2001

Initial mapping and interpretation of lunar crustal magnetic anomalies using Lunar Prospector magnetometer data

L. L. Hood,[1] A. Zakharian,[2] J. Halekas,[3] D. L. Mitchell,[3]
R. P. Lin,[3] M. H. Acuña,[4] and A. B. Binder[5]

Abstract. Maps of relatively strong crustal magnetic field anomalies detected at low altitudes with the magnetometer instrument on Lunar Prospector are presented. On the lunar nearside, relatively strong anomalies are mapped over the Reiner Gamma Formation on western Oceanus Procellarum and over the Rima Sirsalis rille on the southwestern border of Oceanus Procellarum. The main Rima Sirsalis anomaly does not correlate well with the rille itself but is centered over an Imbrian-aged smooth plains unit interpreted as primary or secondary basin ejecta. The stronger Reiner Gamma anomalies correlate with the locations of both the main Reiner Gamma albedo marking and its northeastward extension. Both the Rima Sirsalis and the Reiner Gamma anomalies are extended in directions approximately radial to the center of the Imbrium basin. This alignment suggests that Imbrium basin ejecta materials (lying in many cases beneath the visible mare surface) are the sources of the nearside anomalies. If so, then the albedo markings associated with the stronger Reiner Gamma anomalies may be consistent with a model involving magnetic shielding of freshly exposed mare materials from the solar wind ion bombardment. Two regions of extensive magnetic anomalies are mapped in regions centered on the Ingenii basin on the south central farside and near the crater Gerasimovic on the southeastern farside. These regions are approximately antipodal to the Imbrium and Crisium basins, respectively. The Imbrium antipode anomaly group is the most areally extensive on the Moon, while the largest anomaly in the Crisium antipode group is the strongest detected by the Lunar Prospector magnetometer. A consideration of the expected antipodal effects of basin-forming impacts as well as a combination of sample data and orbital measurements on the nearside leads to the conclusion that the most probable sources of magnetic anomalies in these two regions are ejecta materials from the respective impacts. In both regions the strongest individual anomalies correlate with swirl-like albedo markings of the Reiner Gamma class visible on available orbital photography.

1. Introduction

Although limited Apollo data have established that the observed lunar magnetic field is due to magnetization of crustal materials, the identities of the sources of crustal magnetic anomalies and the nature of the original magnetizing field(s) remain only partially understood (for a review, see *Hood* [1995]). This lack of complete understanding has hampered applications of lunar paleomagnetism for more general geophysical purposes. For example, one potential application of lunar crustal field data is to test the hypothesis that Imbrium basin ejecta is present near the Imbrium antipode in the northwestern portion of the lunar South Pole–Aitken basin [*Haskin*, 1998]. *Lawrence et al.* [2000] have recently presented an analysis of Lunar Prospector thorium and magnetic field data that supports this hypothesis. However, the analysis depends on the assumption that magnetic anomalies in the region are due to magnetized ejecta material from the Imbrium impact. Further work is therefore needed to establish the validity of this and other interpretations of lunar crustal paleomagnetism. The recently obtained Lunar Prospector

[1]Lunar and Planetary Laboratory, University of Arizona, Tucson, Arizona.
[2]Center for Mathematical Sciences, University of Arizona, Tucson, Arizona.
[3]Space Science Laboratory, University of California, Berkeley, California.
[4]Goddard Space Flight Center, Greenbelt, Maryland.
[5]Lunar Research Institute, Tucson, Arizona.

Paper number 2000JE001366.
0148-0227/01/2000JE001366$09.00

magnetometer and electron reflectometer measurements provide an important new database for this purpose.

Earlier work using Apollo data has suggested that ejecta materials, especially basin ejecta, are the most probable sources of lunar orbital magnetic anomalies [*Strangway et al.*, 1973a; *Hood et al.*, 1979a, 1979b; *Anderson and Wilhelms*, 1979]. For example, the Fra Mauro and Cayley Formations, interpreted as primary and secondary ejecta peripheral to the Imbrium basin, were found to be associated with medium-amplitude magnetic anomalies detected with the magnetometer on the Apollo 16 subsatellite [*Hood et al.*, 1979a, 1979b]. Recent analyses of Lunar Prospector electron reflection data have also demonstrated a correlation between magnetic anomalies on the lunar nearside and the Fra Mauro and Cayley Formations [*Halekas et al.*, 2000a]. These results are consistent with sample studies which show that microscopic metallic iron particles are the main ferromagnetic carriers in the reducing lunar environment [*Strangway et al.*, 1973b; *Fuller*, 1974]. Metallic iron particles in lunar materials are typically produced by impact shock reduction of preexisting ferromagnesian silicates and are most abundant in impact-generated breccias. On the other hand, the apparent correlation of one group of magnetic anomalies on the lunar nearside with an extensional graben (Rima Sirsalis) [*Anderson et al.*, 1977] has led to suggestions that subsurface igneous intrusions could be the sources of some anomalies [*Srnka et al.*, 1979]. The latter possibility is not consistent with the general weakness of orbital anomalies over the nearside maria and the near absence of microscopic iron in mare basalt samples. Nevertheless, additional work is needed to establish more completely the most probable sources of orbital anomalies in general and of the Rima Sirsalis anomalies in particular.

Previous work has also indicated that the most probable sources of the ancient lunar magnetizing fields were (1) a former core dynamo during a high-field epoch identified by sample paleointensity studies in the ~3.6– to 3.8–Gyr time interval [*Cisowski et al.*, 1983; *Fuller and Cisowski*, 1987] and (2) transient magnetic fields generated by interaction of impact plasmas with the ambient field during the brief periods when ejecta materials were emplaced [*Hide*, 1972; *Hood and Vickery*, 1984; *Hood and Huang*, 1991]. The importance of the transient field component is indicated by a number of observations. For example, separate exposures of the Fra Mauro Formation south of Imbrium on the lunar nearside are magnetized in very different directions, suggesting a nonsteady, nonuniform magnetizing field [*Hood*, 1980]. In addition, limited Apollo crustal field maps showed that the largest magnetization concentrations do not occur peripheral to lunar impact basins, where ejecta deposits are thickest, but instead occur in regions diametrically opposite (antipodal) to these basins [*Lin et al.*, 1988]. Four relatively young basins (Imbrium, Orientale, Serenitatis, and Crisium) formed during the 3.6– to 3.8–Gyr high-field epoch and have the most distinct antipodal magnetization signatures. A model for the formation of these magnetization enhancements, involving the compression of ambient fields at the antipode by massive impact plasma clouds produced in basin-forming impacts, has been proposed and partially developed theoretically [*Hood*, 1987; *Hood and Huang*, 1991]. However, more detailed measurements in basin antipode regions as well as improved numerical simulations are needed to establish more fully the validity of this proposed mechanism.

One alternative to the core dynamo/basin impact plasma model for the origin of lunar magnetizing fields is that transient fields were generated during cometary impacts onto the lunar surface through the compression of interplanetary magnetic fields by the ionized cometary atmosphere [*Gold and Soter*, 1976]. This possibility received some support from a correlation of a strong magnetic anomaly on the lunar nearside with an unusual albedo marking, Reiner Gamma, interpreted by *Schultz and Srnka* [1980] to represent a region of surface scouring by a recent (<100-Myr-old) cometary impact. However, the origin of the Reiner Gamma albedo markings (and other similar albedo markings elsewhere on the Moon) remains controversial. It has also been proposed that they represent areas whose albedos have been preserved against optical maturation (darkening with time) through the deflection of solar wind ion fluxes by the associated relatively strong magnetic anomalies [*Hood and Schubert*, 1980; *Hood and Williams*, 1989].

Optical maturation, or "space weathering," is a process that darkens and reddens exposed silicate surfaces in the inner solar system (Moon, Mercury, asteroids), thereby weakening mineral absorption bands and complicating compositional interpretations of reflectance spectra [*Pieters et al.*, 1993]. The disappearance with time of bright lunar crater rays is a well-known effect of optical maturation, for instance. Historically, both micrometeoroid impacts and solar wind ion bombardment have been considered as contributors to the production of nanophase iron metal on grain surfaces that leads to the observed maturation [*Housley*, 1977; *Keller et al.*, 1999]. For example, in the case of the ion bombardment, the resulting implantation of solar wind hydrogen may act as an effective reducing agent that enhances the rate of production of nanophase metal from preexisting silicates during micrometeoroid impacts [*Lucey et al.*, 1998]. In addition, solar wind ion sputtering may contribute to vapor deposition of lunar patinas, which are coatings or discolorations caused by space weathering [*Wentworth et al.*, 1999]. The solar wind deflection model for the origin of the lunar swirls predicts that their curvilinear shapes may be at least partly a result of the geometry of ion deflections in a complex, near-surface magnetic field, a possibility supported by numerical ion trajectory simulations [*Hood and Williams*, 1989]. Verification of this model would provide important independent macroscopic evidence for a significant solar wind component of the optical maturation process.

In this paper we report progress toward direct mapping and interpretation of lunar crustal magnetic fields using the magnetometer instrument on Lunar Prospector. In section 2 the methods adopted for data selection and field mapping are described. In section 3, two relatively strong magnetic anomaly groups (the Reiner Gamma group and the Rima Sirsalis group) detected during a brief interval of low-altitude passes across the nearside are mapped and compared in detail with surface geology. In section 4 the most probable sources of the Rima Sirsalis and Reiner Gamma anomalies are evaluated on the basis of a combination of sample data, correlations with surface geology, and the orientation of linear anomalies. In section 5, two extensive groups of strong anomalies on the lunar farside located approximately antipodal to the Imbrium and Crisium basins are mapped and comparisons are made with surface geology. In section 6 the most probable sources of these antipodal anomaly groups are considered on the basis of returned sample data, evidence for anomaly sources elsewhere on the Moon, and theoretical models for antipodal effects of basin-forming impacts. The solar wind deflection model of swirl origins is tested further by comparing the locations of strong individual anomalies in basin antipodal zones with those of swirl-like albedo markings of the Reiner Gamma class. A summary of the main results and conclusions is given in section 7.

2. Data Selection and Field Mapping

The Lunar Prospector spacecraft, launched on January 6, 1998, completed a 19-month orbital mapping mission on July 31, 1999 [*Binder et al.*, 1998]. The first year of the mission was spent at a nominal 100-km altitude to allow optimal surface compositional mapping. However, during the final ~6 months the orbit periapsis was purposely lowered to the 15- to 30-km range to allow improved mapping of crustal magnetic and gravity fields. Because of the near-polar orbit, useful coverage of the Moon was substantially improved relative to that obtained during the Apollo missions. Two instruments on the Lunar Prospector spacecraft are designed to measure lunar crustal fields. The magnetometer measures the vector field directly at the spacecraft altitude, while the electron reflectometer measures the surface field indirectly by determining the ratio of reflected to incident low-energy electrons. Initial results were reported by *Lin et al.* [1998].

The methods for data selection and field mapping using Lunar Prospector magnetometer data follow closely those that were developed for application to Apollo 15 and 16 subsatellite magnetometer data [*Russell et al.*, 1975; *Hood et al.*, 1981]. Four steps in the mapping procedure are outlined as follows:

1. In order to allow detection of relatively weak lunar crustal magnetic fields, it was first necessary to select time intervals for analysis when solar wind plasma densities were low and when field variations of external origin were minimal. Two environments of this type were identified. First, times when the Moon was in the relatively undisturbed plasma environment of the geomagnetic tail lobes were most ideal for mapping lunar fields at all points along the spacecraft orbit. Second, times when the Moon was in the solar wind but the spacecraft was in the lunar wake were also found to be useful for mapping lunar fields. However, because temporally variable plasma disturbances do occur both in the tail lobes and in the solar wind wake, it was necessary to visually examine each orbit so that only undisturbed time intervals were selected.

2. The magnetometer data were transformed into a lunar radial, east, and north coordinate system along each orbit. A data file for each orbit was then constructed containing the three field components, the spacecraft altitude, selenographic latitude, and longitude for each measurement point. Remaining low-frequency external field contributions were next minimized by least squares fitting and removing a suitable (quadratic) polynomial function for each field component and for each orbit. The crustal field magnitude (B total) was then calculated as the square root of the sum of squares of the three detrended field components.

3. Because of the strong altitude dependence of lunar crustal fields, only the lowest-altitude portions of each orbit were considered, and true lunar fields were distinguished from remaining external field disturbances by their repetition on successive orbit passes. The radial field component was most useful for final editing since this component is less susceptible to external field variations. The latter property is a consequence of the conservation of the normal component of the magnetic field at the surface of a conducting sphere.

4. Two-dimensional filtering of individual orbit data segments using a moving boxcar algorithm was applied to produce a vector magnetic field map along the curved surface defined by the spacecraft altitude. For the maps presented here, the weights in the 5×5 boxcar were equal, the dimensions of the boxcar were $1.25° \times 1.25°$, and the algorithm was applied twice in succession to the binned data. The effective minimum wavelength of mapped anomalies is therefore $\sim 2.5°$. Maps of the three field components (radial, east, and north), the field magnitude, and the spacecraft altitude were constructed in this manner. In this paper, only maps of the field magnitude are shown since this scalar quantity correlates most closely in location with magnetic anomaly sources at or below the lunar surface.

For the purpose of initial mapping and interpretation of the strongest lunar magnetic anomalies, we have selected data from three time periods during the final low-altitude phase of the Lunar Prospector mission. These periods were days 81–82, days 173–175, and days 141–142 of 1999. During each of these periods, plasma-related disturbances were minimal, the spacecraft altitude was relatively low, and the selenographic region coincided with the locations of especially strong magnetic anomalies as identified by repetition on successive orbit passes. Data from days 81–82 of 1999 were se-

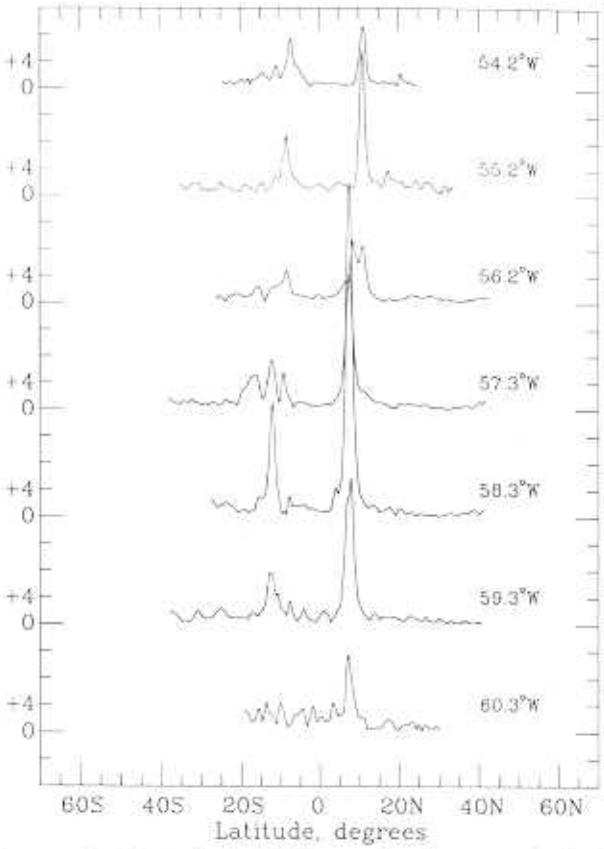

Figure 1. Plot of the field magnitude versus latitude for a series of Lunar Prospector passes across the western nearside occurring on days 81–82 of 1999. The spacecraft altitude ranged from approximately 18 to 20 km along these traverses. The spacecraft longitude at the equator is given at the right of each orbital field plot.

lected from times when the Moon was in the solar wind and the spacecraft was in the lunar wake. Coverage was across a portion of the western lunar nearside including the Reiner Gamma region on western Oceanus Procellarum. Data from days 173–175 and days 141-142 of 1999 were selected from times when the Moon was in the geomagnetic tail. Coverage was across portions of the lunar farside including the areas antipodal to the Imbrium and Crisium basins.

3. Reiner Gamma and Rima Sirsalis Anomalies

Figure 1 is a plot of the field magnitude (the square root of the sum of squares of the three field components) versus latitude for a series of passes across the western nearside occurring on days 81–82 of 1999. During these passes the spacecraft altitude ranged from approximately 18 to 20 km, and the orbit track separation at the equator was ~30 km (~1° of longitude). Two groups of anomalies are present centered on latitudes of approximately 8°N and 10°S. The northern group correlates with the Reiner Gamma albedo marking on western Oceanus Procellarum as mapped previously using Apollo 16 subsatellite magnetometer data [*Hood et al.*, 1979a, 1979b]. The southern group occurs near the location of Rima Sirsalis, an extensional graben, and was first identified using electron reflection data by *Anderson et al.* [1977].

Application of a two-dimensional filtering algorithm to the field magnitude data of Figure 1 for the northern anomaly group yields the contour map shown in Figure 2. As described in section 2, the filtering program first sorts the data into 0.25° × 0.25° bins and smooths two-dimensionally using a 5 × 5 moving boxcar method. The contour map of Figure 2 is superposed onto a composite of Lunar Orbiter IV photographs of western Oceanus Procellarum showing the Reiner Gamma albedo marking and the 30-km-diameter crater Reiner. Unlike maps constructed from the Apollo 16 subsatellite magnetometer data, this map extends over the entire region of albedo markings north of 3°N latitude. However, the resolution of the map is limited in the east-west direction by the 30-km orbit track separation.

While the Apollo data demonstrated a correlation of the main southern albedo marking (7.5°N, 58.5°W) with the largest single anomaly of the northern group, the Prospector data show that a smaller anomaly is centered approximately on the largest secondary albedo marking (11°N, 55°W). The anomaly group is also generally extended parallel to the trend of the albedo marking distribution.

Two-dimensional filtering of the field magnitude data of Figure 1 for the southern anomaly group yields the contour map shown in Plate 1. This map is superposed onto a geologic map of the Grimaldi quadrangle [*McCauley*, 1973]. The largest single anomaly is centered just southeast of the Rima Sirsalis rille, an extensional graben oriented nearly radial to the Imbrium basin. As noted in section 1, this anomaly and its proximity to Rima Sirsalis were initially reported by *Anderson et al.* [1977] on the basis of Apollo electron reflection data. The second anomaly of Plate 1 is located over the adjacent mare surface and does not correlate with any single surface feature.

4. Interpretation of the Nearside Anomalies

For the purpose of investigating likely sources of the Reiner Gamma and Rima Sirsalis anomalies, it is preferable to consider first the Rima Sirsalis anomalies. A clear correlation of these anomalies with the rille itself would suggest a deep-seated source such as igneous intrusions [*Srnka et al.*, 1979]. However, the data of Plate 1 do not support a direct correlation with the rille. The main anomaly is centered at 58.2°W, 12.0°S. This location is just southeast of the rille and coincides approximately with the center of an Imbrian-aged smooth plains unit (designated as Ip by McCauley). The latter unit is interpreted here as a probable deposit of primary or secondary basin ejecta analogous to the Cayley Formation. Given the known tendency for impact breccias and soils to contain relatively large amounts

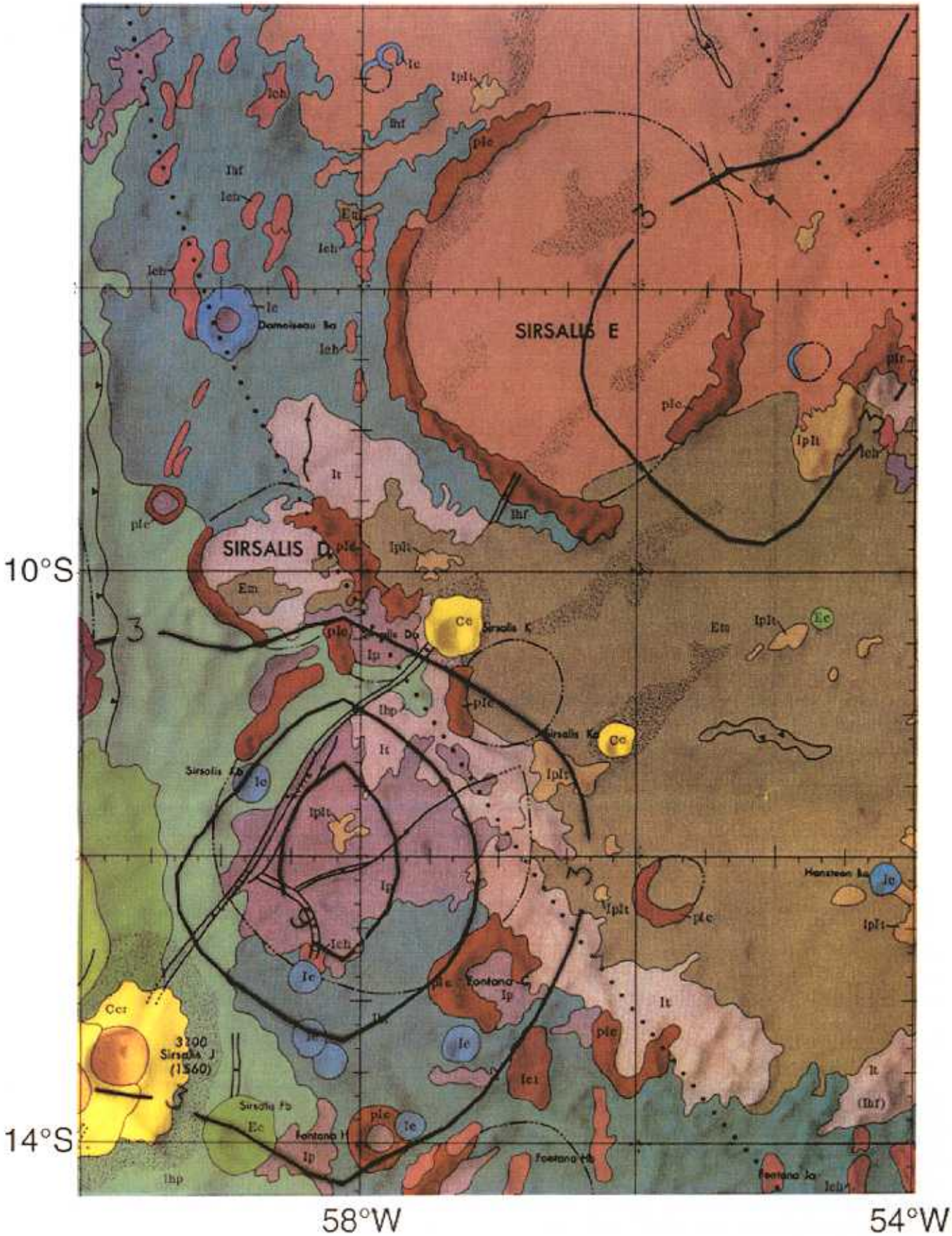

Plate 1. Superposition of a contour map of the field magnitude over the Rima Sirsalis region onto a geologic map of the Grimaldi quadrangle [*McCauley*, 1973]. The contour interval is 3 nT. Rima Sirsalis, an extensional graben, is indicated by parallel lines striking southwest to northeast across the diagram.

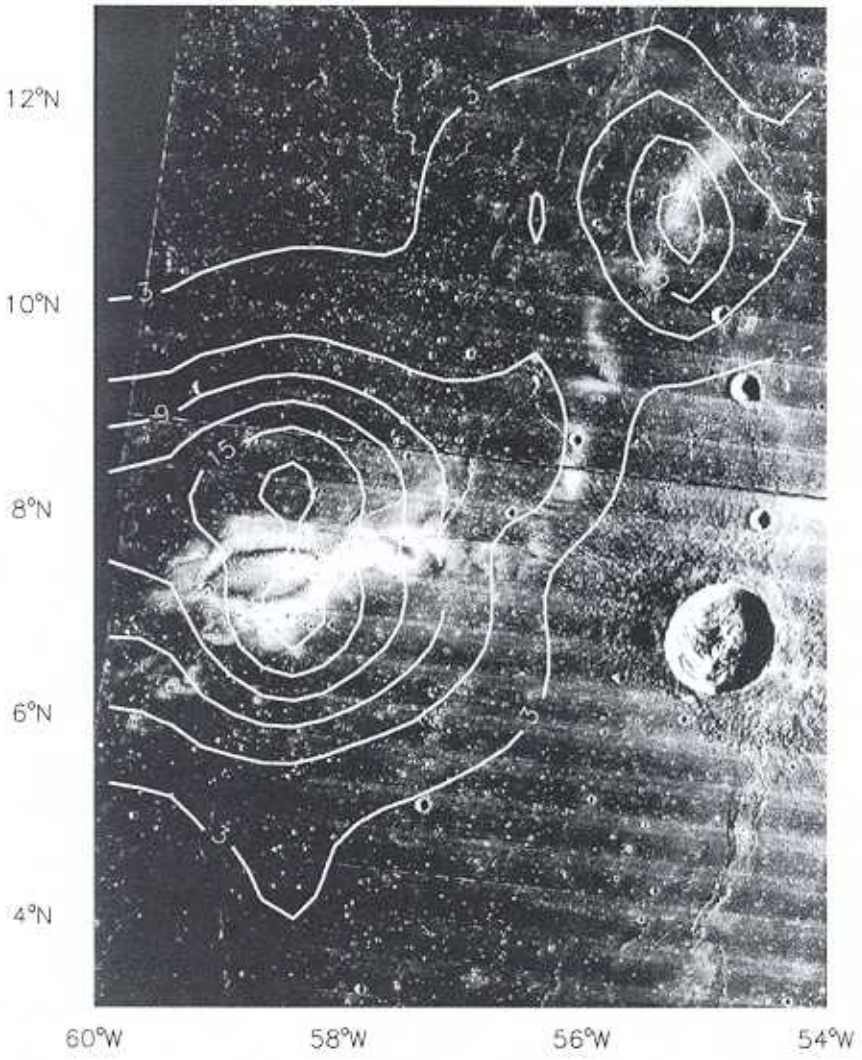

Figure 2. Contour map of the field magnitude over the Reiner Gamma region on western Oceanus Procellarum constructed from the orbit segments of Figure 1. The contour interval is 3 nT and the 30-km crater Reiner is at the lower right.

of microscopic metallic iron in the single domain size range and given the known association of the Cayley Formation with orbital anomalies, it is suggested that this smooth plains unit is the most probable source of the main Rima Sirsalis anomaly. The absence of other electron reflection anomalies on the nearside that correlate with rilles [*Halekas et al.*, 2000a] is consistent with this interpretation.

The secondary Rima Sirsalis anomaly (centered at 55.5°W, 8.5°S) is centered over the southeastern section of Sirsalis E in a region dominated by mare basalt. It is therefore unlikely that the anomaly source is at the surface, but it may lie beneath the thin veneer of weakly magnetic mare material. The possibility of a subsurface source of this secondary anomaly was noted previously by *Anderson et al.* [1977], who suggested that the source may be an extension of the rille, covered up by subsequent lava flows. If the Cayley-like Imbrian plains unit is the actual source of the main anomaly, then it may be proposed that a similar buried unit is responsible for the secondary anomaly. The possibility of anomaly sources beneath the visible mare is supported also by earlier studies of the Fra Mauro Formation anomalies south of the crater Kepler. Some of the latter anomalies are present over the smooth maria in addition to being present over visible exposures of the Fra Mauro [see *Hood*, 1980, Figure 4].

An additional property of the Rima Sirsalis anomalies that suggests an Imbrium basin–related origin is their orientation approximately radial to the center of Imbrium. Some visible exposures of the Fra Mauro and Cayley Formations tend to be oriented radial to Imbrium as expected from their fluidized state and low angles of incidence immediately after the basin-forming event. Therefore the alignment of the Rima Sirsalis anomalies radial to Imbrium does not necessarily imply an association with the rille itself. Also, preliminary studies of the vector components of the field over Rima Sirsalis indicate a similar bulk direction of magnetization for both the primary and secondary Rima Sirsalis

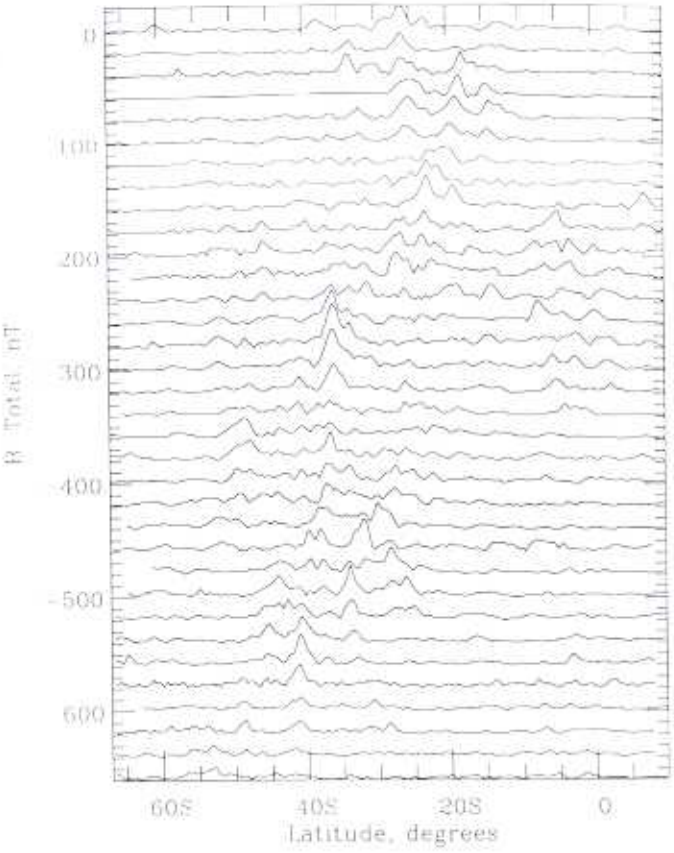

Figure 3. Compressed vertical scale plot of field magnitude anomalies detected along a series of orbits (1231-1264) across the south central farside on days 173–175 of 1999. The spacecraft altitude ranged from 18 to 22 km. All field values are positive, and the vertical scale is 10 nT per division.

anomalies. This would be consistent with rapid emplacement in a relatively uniform magnetic field.

The close correlation of the anomalies of Figure 2 with the Reiner Gamma albedo marking raises again the issue of the origin of the lunar swirls. As stated in section 1, two major models for the origin of the swirls have been proposed since the discovery of the Reiner Gamma anomaly: the cometary impact model [*Schultz and Srnka*, 1980] and the solar wind deflection model [*Hood and Schubert*, 1980; *Hood and Williams*, 1989]. Detailed spectral reflectance studies of Reiner Gamma, the only swirl accessible to ground-based remote-sensing studies, have suggested that it has a surface composition consisting of a mixture of fresh highlands materials with much greater amounts of local mare basalt [*Bell and Hawke*, 1981]. No significant amounts of compositionally anomalous (i.e., cometary) materials were detectable. It was therefore concluded that optical remote-sensing data do not strongly discriminate between the two models.

The most probable sources of the Reiner Gamma anomalies of Figure 2 are quite different depending on whether the cometary impact model or the solar wind deflection model is assumed to be valid. If the cometary impact model is adopted, then the most probable sources of the anomalies are thin layers of uppermost regolith coinciding with the visible swirls. If the solar wind deflection model is adopted, then the most probable sources are beneath the visible mare surface. The correlation of both the primary and secondary anomalies of Figure 2 with swirl locations is supportive of the solar wind deflection model but does not necessarily exclude the cometary impact model. There is one characteristic of the Reiner Gamma anomalies that suggests subsurface sources in the form of basin ejecta: The anomalies are aligned nearly radial to the center of Imbrium. By analogy with the Rima Sirsalis and Fra Mauro anomalies, this orientation suggests that Imbrium basin ejecta units may be the sources. In this regard, it should be mentioned that ejecta lying beneath the visible mare surface would not have been easily thermally demagnetized by the mare basalt flows. For thermal diffusivities characteristic of lunar materials it can be shown that only the upper few meters of ejecta would have been exposed to temperatures exceeding the Curie temperature for metallic iron unless the basalt flow was >>1 km thick.

Even if a subsurface Imbrium ejecta model for the sources of the Reiner Gamma anomalies is correct, such an interpretation does not directly verify the solar wind deflection model for swirl origins. No absolute proof of the deflection model is likely to be possible without independent future measurements. For example, future surface traverses across the Reiner Gamma Formation with a roving vehicle carrying both a magnetometer and an energetic charged particle detector would most clearly demonstrate the solar wind deflection model. In the meantime, further analysis of Lunar Prospector electron reflectometer data from low-altitude passes over the strongest anomalies may be useful in obtaining indirect evidence for surface shielding by lunar fields.

The extended "tail" of the Reiner Gamma Formation is especially enigmatic and seems difficult to explain in terms of either the cometary impact model or the solar wind deflection model. If the solar wind deflection model is assumed to be valid, then some additional process must have been involved to explain the overall morphology of Reiner Gamma. One possibility is that secondary impacts from the nearby Eratosthenian crater Cavalerius may have been responsible for producing fresh mare material whose albedos were then selectively preserved by the underlying strong magnetic field sources [*Hood et al.*, 1979b].

5. Imbrium and Crisium Antipode Anomalies

Much more extensive groups of magnetic anomalies comparable to or larger in amplitude than the Reiner Gamma and Rima Sirsalis anomalies were detected on the lunar farside by both the magnetometer and electron reflectometer on Lunar Prospector. Figure 3 is a compressed time series plot of the field magnitude versus latitude measured along a series of orbits on days

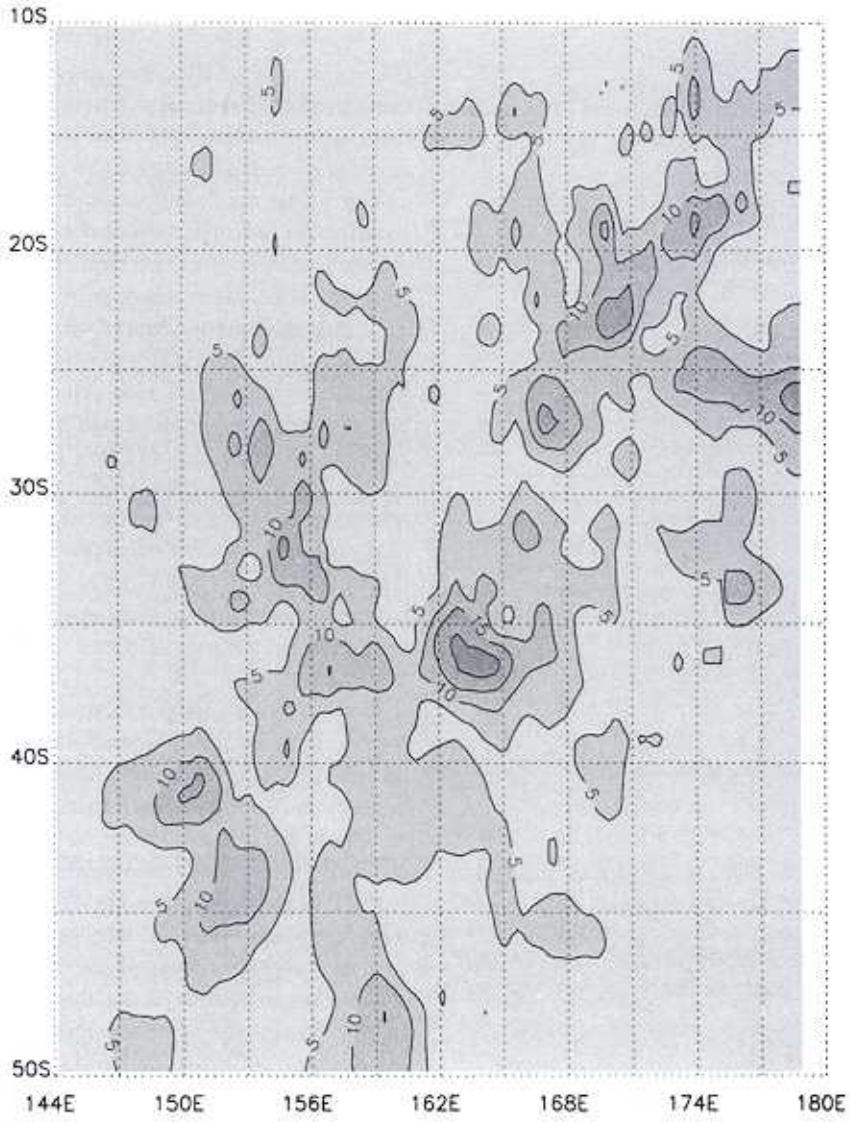

Figure 4. Contour map of the magnetic field magnitude constructed from the orbit passes of Figure 3. The contour interval is 5 nT.

173–175 of 1999. (Note that the vertical scale is much smaller than for Figure 1.) The repeating patterns identify the field anomalies as being of lunar crustal origin. The spacecraft altitude during these orbit passes ranged from 18 to 22 km. The largest single anomaly has an amplitude (>30 nT) at 19-km altitude and is comparable to that of the strongest Reiner Gamma field anomaly shown in Figure 1. However, this group of anomalies is much larger in areal extent and number than the near-side anomalies of Figure 1. Comparisons with near-global maps of the distribution of surface fields produced by the electron reflection method show that this group of anomalies, located in a region centered on and surrounding the Ingenii basin on the south central far-side, is the largest of its kind on the Moon. Because of its position centered near the antipode of the Imbrium basin, we will refer to these anomalies as the Imbrium antipode anomalies.

Figure 4 is a contour map of the Imbrium antipode anomalies after two-dimensional filtering in the same manner as described in relation to Figure 2 and Plate 1. Seven to eight smoothed maxima on the map exceed 15 nT at the spacecraft altitude (ranging from 18 to 22 km) and are distributed over a region comparable in size to the Imbrium basin itself. Plate 2 is a partial geologic map of the Mare Ingenii region near the Imbrium antipode on which has been superposed a contour map of the largest single magnetic anomaly detected by the Lunar Prospector magnetometer in this region. The major geologic units are traced from *Stuart-Alexander* [1978]. Figure 5 is a corresponding enlargement of Lunar Orbiter II photograph 75M showing the pre-Nectarian aged Ingenii basin with mare basalt fill and superposed swirls. The blue shading in Plate 2 indicates the occurrence of unusual grooved terrain (see especially the basin walls in Figure 5) that has been in-

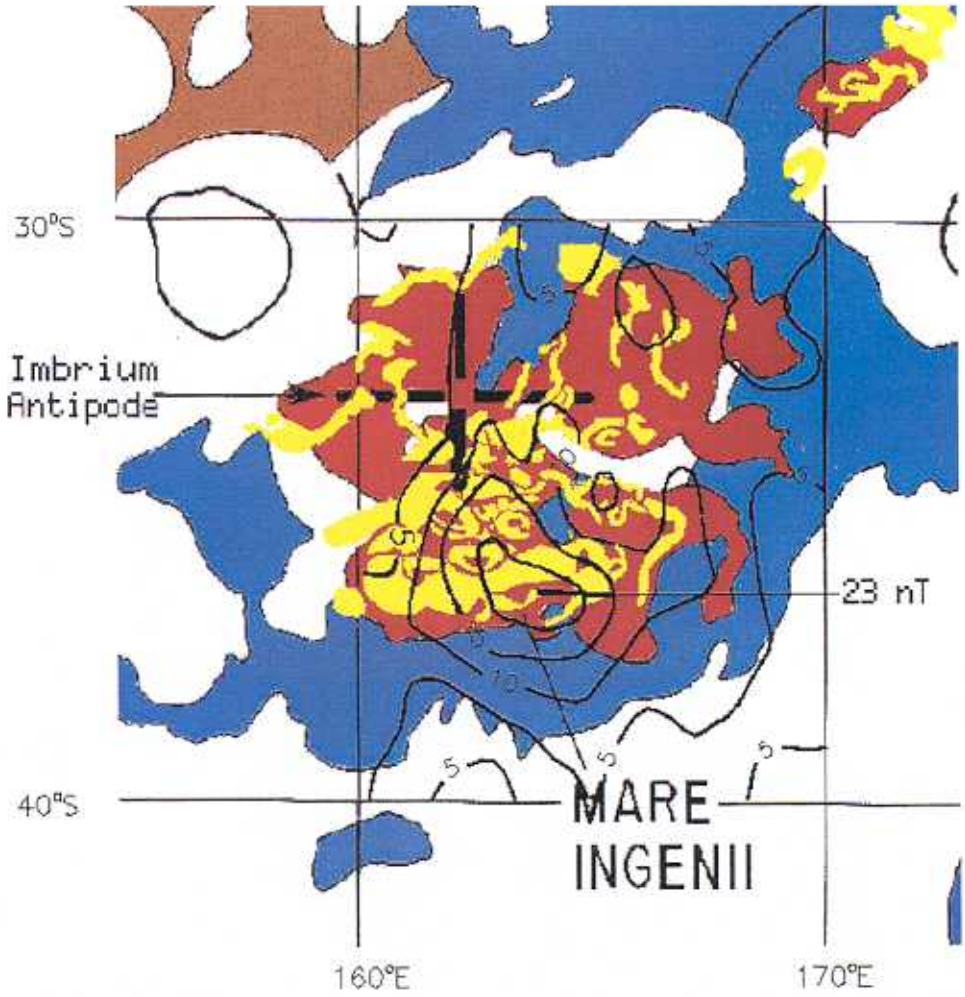

Plate 2. Contour map of the magnetic field magnitude over the Mare Ingenii region on the south central farside. The contour interval is 5 nT. Older Pre-Nectarian terrain is indicated by brown shading; unusual grooved and lineated terrain is indicated by blue shading; and areas dominated by mare basalt are shaded red. The locations of swirl-like albedo markings of the Reiner Gamma class are sketched in yellow. Geologic units are taken from *Stuart-Alexander* [1978].

terpreted as originating via the convergence of seismic compressional waves at the time of the Imbrium impact [*Schultz and Gault*, 1975]. This terrain clearly dates from the time of the Imbrium impact although its origin remains incompletely determined. The red shading indicates later (postimpact) mare basalt filling of the Ingenii basin, while the yellow markings indicate the occurrence of probable swirls as seen also in Figure 5. The smoothed anomaly maximum of 23 nT occurs at a mean altitude of ~19 km. The anomaly peak is centered approximately on the most visible group of swirls.

The strongest single anomaly derived thus far from Lunar Prospector magnetometer data is part of a cluster of anomalies centered near the antipode of the Crisium basin. A compressed time series plot of the field magnitude measured along a series of orbits on days 141 and 142 of 1999 is shown in Figure 6. The largest single anomaly has an amplitude of nearly 40 nT at an altitude of 24 km, significantly higher than the 18– to 19–km minimum altitudes at which the Imbrium antipode and Reiner Gamma/Rima Sirsalis anomalies were measured. This anomaly cluster, while larger in areal extent than the Reiner Gamma anomalies, is smaller than that of the Imbrium antipode anomalies. These "Crisium antipode" anomalies were mapped previously at much higher altitudes using Apollo 15 subsatellite magnetometer data [*Hood*, 1981] and are located over pre-Nectarian terrain including the crater Gerasimovic just west of the main ejecta facies of the Orientale basin [*Hood and Williams*, 1989]. Curvilinear albedo markings interpreted to be of the Reiner Gamma class are visible on a former Soviet Zond 8 photograph of the region (Figure 7).

Two-dimensional filtering of the data of Figure 6 yields the contour map shown in Plate 3 superposed on a partial geologic map based on an original map of the lunar east side by *Wilhelms and El-Baz* [1977]. The largest single magnetic anomaly has a smoothed amplitude of 26 nT, while secondary anomalies with amplitudes of 18 and 16 nT are also present. This cluster

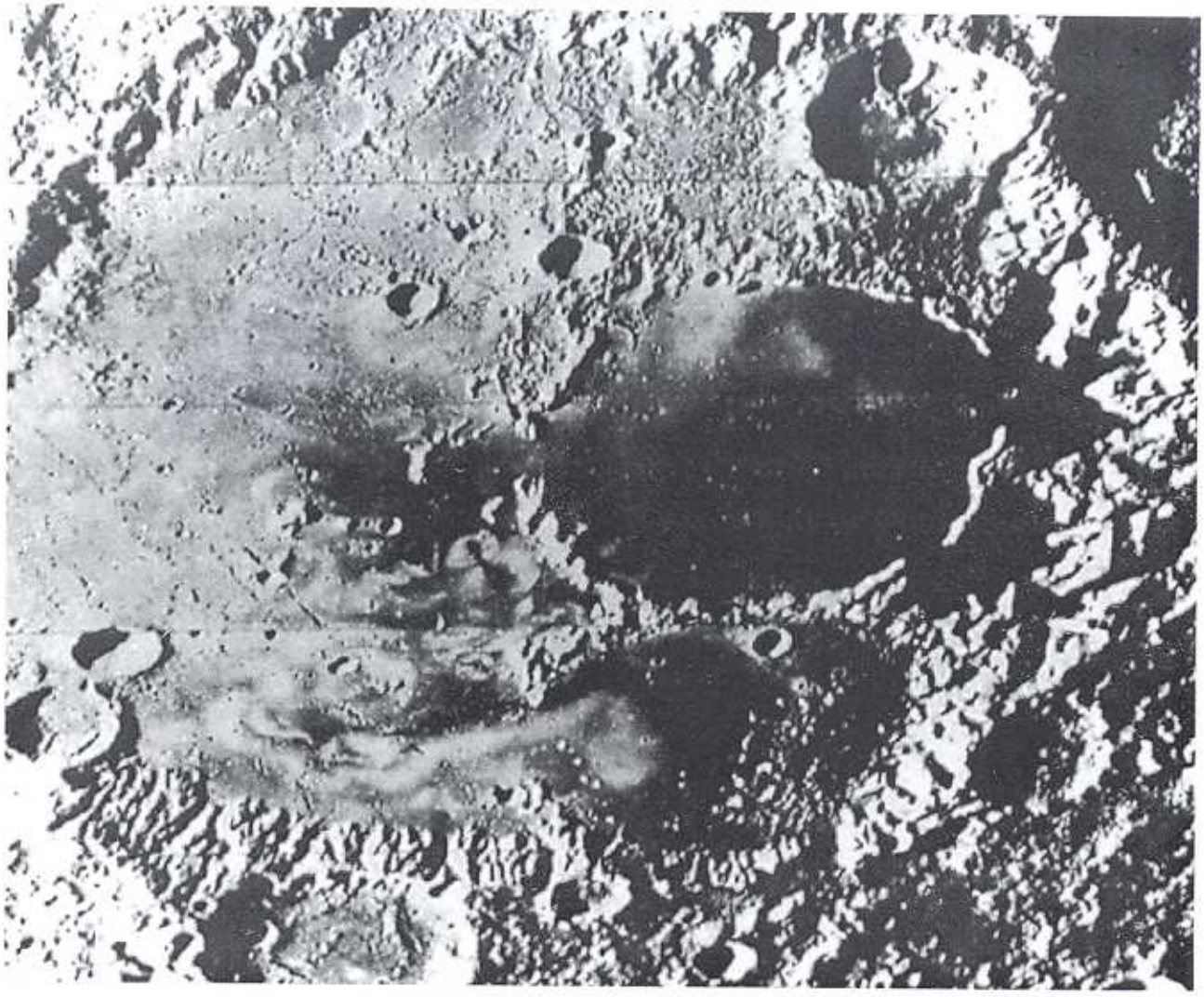

Figure 5. Portion of Lunar Orbiter II photograph 75M showing the pre-Nectarian aged Ingenii basin with mare basalt fill and superposed swirls. Note the grooved and lineated terrain along the southern basin walls. The 50-km crater Zelinski is at top right.

of anomalies is centered approximately at 123°E, 23°S, on the main group of swirls mapped previously [*Schultz and Srnka*, 1980; *Hood and Williams*, 1989].

6. Interpretation of the Farside Anomalies

The extensive groups of strong anomalies mapped thus far on the lunar farside occur near to the antipodes of two young large basins, Imbrium and Crisium. The Imbrium antipode region is characterized by the largest areal distribution of strong anomalies on the Moon, while the Crisium antipode region is characterized by the strongest single anomaly yet mapped on either the nearside or the farside. In both cases the strongest individual anomalies tend to correlate in position with swirl-like albedo markings of the Reiner Gamma class. These results represent a significant improvement over earlier analyses of lower-resolution Apollo electron reflection data over the same regions [*Hood and Williams*, 1989].

With respect to the Imbrium antipode anomalies, the geologic complexity of the region makes the identification of anomaly sources difficult. Although no surface geologic unit in the Ingenii region is specifically designated as basin ejecta, calculations of the distribution of ejecta from a basin-scale lunar impact [*Moore et al.*, 1974] show that a moderate enhancement occurs in the antipode region. It is therefore likely that Imbrium ejecta exists in this region in spite of the obscuring complex topography and later basalt flooding episodes. On the basis of the magnetic weakness of mare basalt samples and comparisons with nearside anomalies, we suggest that the source of this largest anomaly may lie beneath the Ingenii mare basalt flows. The correlation of the strongest anomaly with the most visible group of swirls supports but does not prove the solar wind deflection model. The absence of clearly recognizable swirls in the adjacent highlands where less intense anomalies were mapped according to Figure 4 does not represent a contradiction of the solar wind deflection model because of the sparsity of orbital photography in this region and

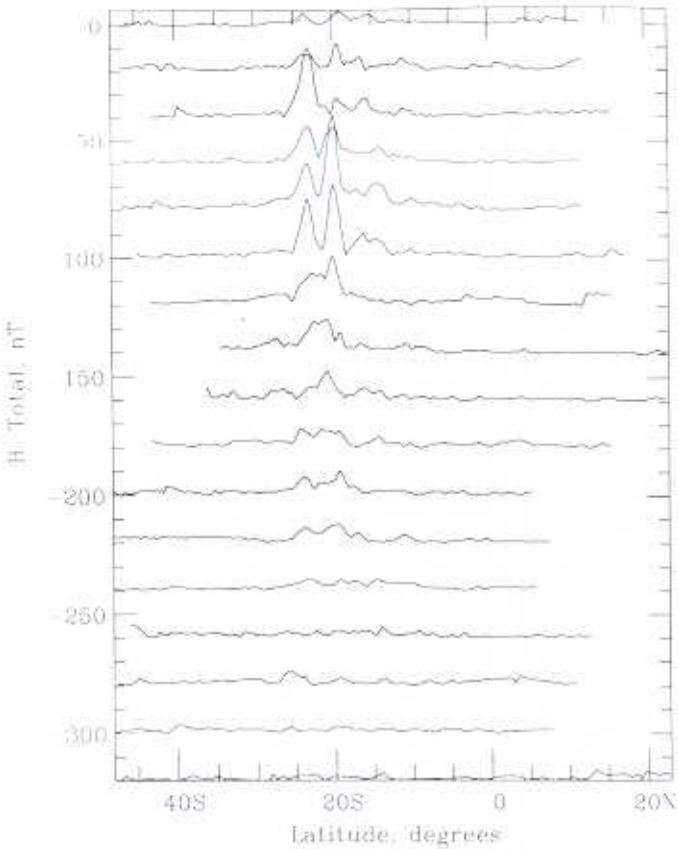

Figure 6. Compressed vertical scale plot of the field magnitude along a series of orbit passes (815-831) across the southeast central farside on days 141–142 of 1999. The vertical scale is 10 nT per division, and all field values are positive.

the general difficulty of recognizing subtle albedo contrasts in the lunar highlands. Swirls are much more easily visible when superposed on mare basalt such as that in Mare Ingenii and within the floor of Van de Graaff crater.

The Crisium antipode region is also not amenable to an easy identification of anomaly sources. Its location near the periphery of the Orientale ejecta field is an additional complication. It can only be suggested on the basis of sample data and likely anomaly sources elsewhere on the Moon that basin ejecta sources are most probable. The correlation of the strongest anomalies with apparent swirls of the Reiner Gamma class adds additional support to the solar wind deflection model. Swirls are visible even in the highlands near the Crisium antipode. Because swirls are strong forward reflectors, this may be a consequence of an unusually favorable solar zenith angle for the Zond 8 photograph of Figure 7. However, it may also be a consequence of a stronger magnetic anomaly capable of more effectively deflecting solar wind ions.

Theoretical predictions of a number of antipodal effects of basin-forming impacts reduce the likelihood that the locations of these two anomaly groups antipodal to Crisium and Imbrium are fortuitous. As noted above, moderate basin ejecta convergence at the antipode is predicted by ballistic calculations on a spherical Moon [*Moore et al.*, 1974]. Seismic modification in the same location is predicted by the analysis of *Schultz and Gault* [1975]. The unusual hilly and lineated terrain (highlighted in blue in Plate 2 and visible on the walls of the Ingenii basin in Figure 5) near the Imbrium antipode has been interpreted by some authors (e.g., Schultz and Gault) as a consequence of the seismic modification process. Magnetic field compression at the antipode by impact-generated plasmas is predicted by the two-dimensional hydrocode calculations of *Hood and Huang* [1991]. The combination of these effects occurring during simultaneous or overlapping time periods could have led to the observed magnetization enhancements. If the model of *Hood and Huang* [1991] for the formation of magnetic anomalies antipodal to lunar impact basins is adopted, then it would follow that the anomaly sources in the two mapped farside regions must have originated at the times of the Imbrium and Crisium impacts. Possible anomaly sources in these regions include both impact ejecta and seismically modified terrain [*Hood and Huang*, 1991]. However, given the sample and nearside orbital evidence for basin ejecta sources elsewhere on the Moon, the most probable sources are considered to be basin ejecta.

If the observed strong farside anomalies have a basin-related origin, then this inference also adds support for the solar wind deflection model for the origin of the lunar swirls. It is unlikely that recent (<100-Myr) cometary impacts would occur by chance preferentially in zones antipodal to large lunar basins dating from the 3.6- to 3.8-Gyr period.

7. Summary and Conclusions

In this paper we have applied methods developed earlier for mapping lunar crustal magnetic fields using Apollo subsatellite magnetometer data in order to produce initial maps of relatively strong anomalies detected at low altitudes with the magnetometer instrument on Lunar Prospector. Maps of the field magnitude were compared with surface geologic maps over a series of regions on both the lunar nearside and farside. On the nearside, two small regions of relatively strong anomalies were mapped over the Reiner Gamma Formation on western Oceanus Procellarum and near Rima Sirsalis, an extensional graben on the southwestern edge of Oceanus Procellarum. On the farside, much larger regions of strong anomalies were mapped in regions centered on the Ingenii basin in the south central highlands and centered near the crater Gerasimovich in the southeastern subequatorial zone. The former region is approximately antipodal to the Imbrium basin, while the latter region is located near to the antipode of the Crisium basin. Our interpretations are guided in part by returned Apollo sample studies and earlier Apollo subsatellite mapping of magnetic anomalies over the Fra Mauro and Cayley Formations south of the Imbrium basin.

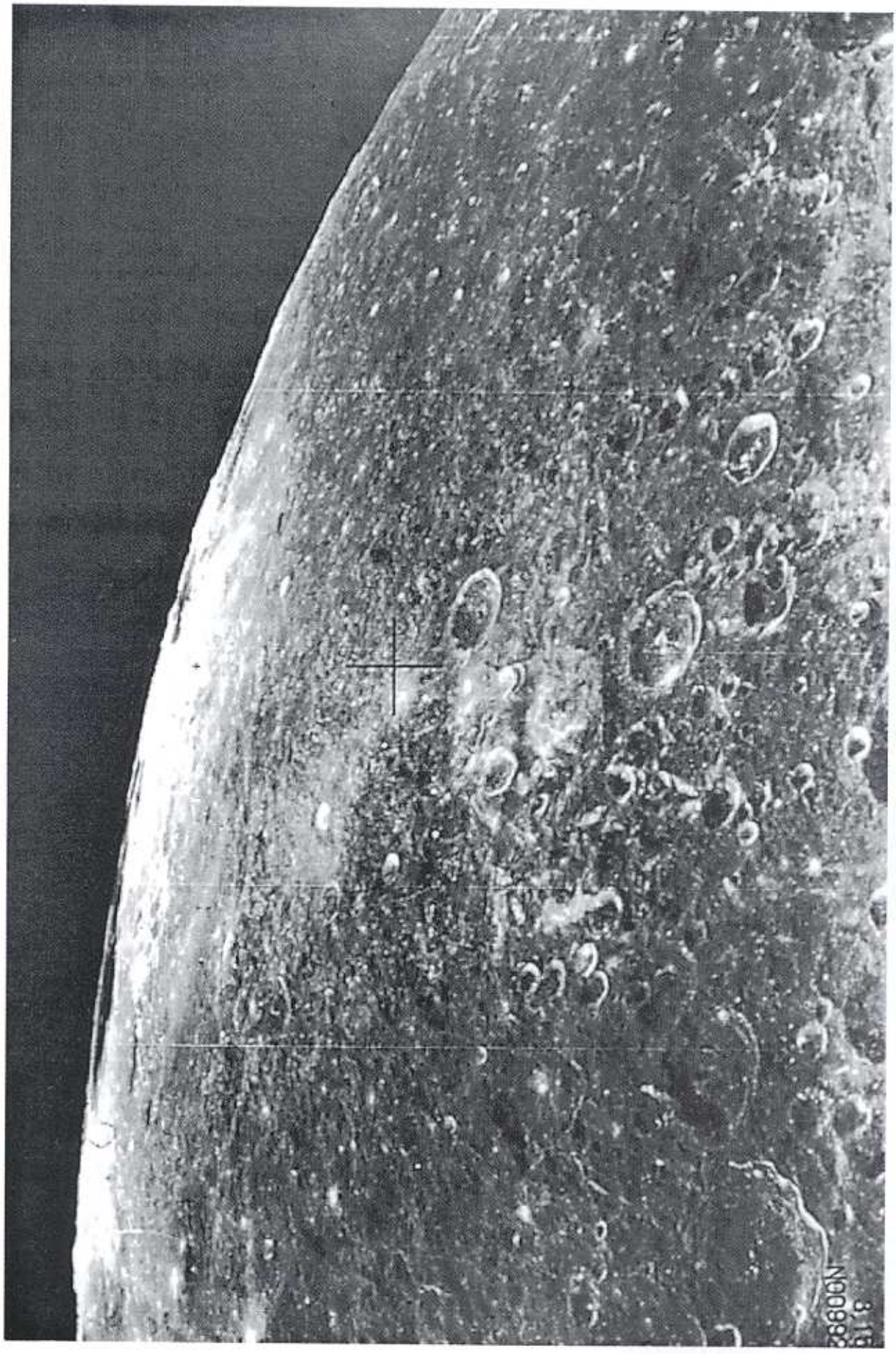

Figure 7. Former Soviet Zond 8 photograph of the southeastern lunar farside. The Orientale basin is on the far horizon and the 80-km-diameter degraded crater Gerasimovich is at center. Swirl-like albedo markings interpreted to be of the Reiner Gamma class [*Schultz and Srnka*, 1980] are visible against the underlying highland terrain.

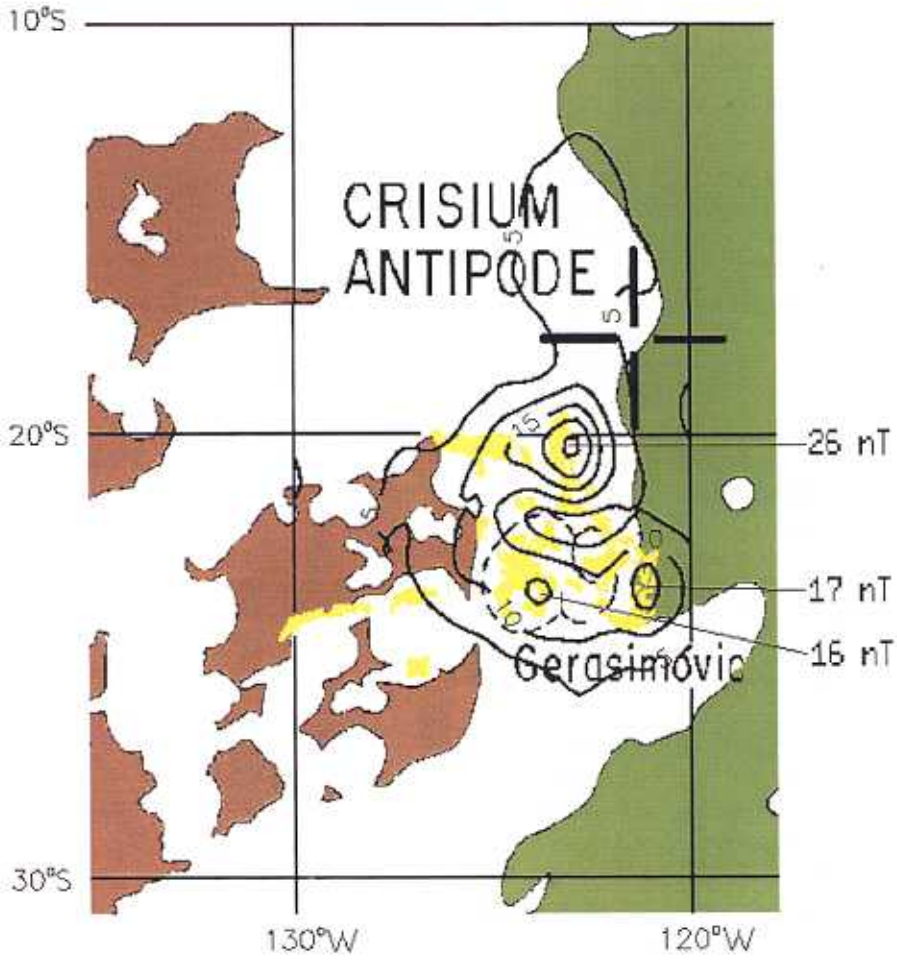

Plate 3. Superposition of a contour map of field magnitude anomalies from Figure 6 onto a partial geologic map of the region near the Crisium antipode (based on original geologic mapping by *Wilhelms and El-Baz* [1977]). The contour interval is 5 nT. Brown shading indicates pre-Nectarian terra, while the locations of swirl-like albedo markings similar to Reiner Gamma are marked in yellow. The outline of the degraded crater Gerasimovic is indicated by a dashed line.

It was found that the main Rima Sirsalis anomaly does not correlate clearly with the rille itself but occurs mainly over an adjacent Imbrian-aged smooth plains unit interpreted as primary or secondary basin ejecta. Such a source would be more consistent with sample data and would remove the need for earlier proposals that subsurface igneous intrusions are the sources of this anomaly. A secondary anomaly east of Rima Sirsalis occurs over a surface region dominated by thin mare basalt flows that are magnetically weak elsewhere on the Moon. The two Rima Sirsalis anomalies are aligned approximately radial to the center of Imbrium. On the basis of sample data and comparisons with other nearside anomalies, it is therefore suggested that the most probable source of the secondary anomaly is a subsurface Imbrian-aged plains unit similar to that which correlates with the main anomaly. The alignment radial to Imbrium may have resulted from low-angle impact of fluidized ejecta subsequent to the basin-forming event. According to impact field amplification models [e.g., *Hood and Vickery*, 1984], magnetization may have occurred in the presence of a complex magnetic field generated at the periphery of a turbulent, expanding plasma cloud originating at the impact site.

In the case of the Reiner Gamma anomalies, both the main anomaly and a secondary anomaly correlate with surficial, curvilinear albedo markings on the mare surface. Like the Rima Sirsalis anomalies, the Reiner Gamma anomalies are oriented radial to Imbrium. We therefore suggest that the most probable sources of the Reiner Gamma anomalies are Imbrium basin ejecta units beneath the visible thin veneer of mare basalt flows. For thermal diffusivities characteristic of lunar materials, such a magnetized ejecta unit could have survived the thermal pulse associated with mare basalt emplacement. If this source model is correct, then the solar wind deflection model for swirl origins would be favored over the cometary impact model. However, an additional process, perhaps involving secondary impacts from the nearby Eratosthenian crater Cavalerius, may have exposed fresh mare material that helped to shape the overall morphology of the Reiner Gamma swirl and its northeastward extension.

If the basin ejecta source model for the nearside

anomalies is accepted, a remaining question is why some ejecta terrains are strongly magnetized and not others. More extensive studies of nearside anomalies using the Lunar Prospector electron reflection data set has shown that while many Cayley-type light plains regions correlate with magnetic anomalies, and overall the light plains are more magnetic than other terrains, by no means are all or even most of the light plains magnetically strong [*Halekas et al.*, 2000a]. Similarly, although some Fra Mauro Formation exposures are magnetically strong, most exposures are magnetically weak. Two possible explanations may be suggested. First, the composition (specifically, metallic iron content) and therefore the magnetic susceptibility may vary from one ejecta terrain to another. In support of this possibility, some of the most clearly magnetized Cayley plains units (those close to the Apollo 16 landing site) have been shown to have unusually high abundances of metallic iron [*Korotev*, 1994]. Second, the transient nature of the magnetic fields generated by a basin-forming impact and their interaction with ejecta may have required a nearly optimal timing and configuration for efficient magnetization acquisition.

The strong magnetic anomaly group in the Imbrium antipode region on the south central farside is the largest in size on the Moon, as verified by recent analyses of global Lunar Prospector electron reflectometer data [*Halekas et al.*, 2000b]. The strongest single anomaly in the Crisium antipode region appears to be the largest in amplitude on the Moon (40 nT at 24–km altitude). The complexity of highland geology in both the Imbrium antipode region and the Crisium antipode region as well as the paucity of high-resolution photography inhibits a direct identification of anomaly sources. The presence of superposed mare basalt plains (e.g., within the Ingenii basin) also increases the difficulty of directly recognizing anomaly sources. Nevertheless, theoretical considerations of the antipodal effects of basin-forming impacts provide some additional constraints. Model calculations predict both a moderate enhancement of ejecta thickness at the antipode [*Moore et al.*, 1974] and shock modification of subsurface terrain by seismic waves generated by the impact [*Schultz and Gault*, 1975]. In addition, plasma physical models predict an amplification of the magnetic field at the antipode shortly after the impact [*Hood and Huang*, 1991]. In principle, both seismically modified terrain and antipodal ejecta may have acquired a magnetization in the presence of an impact-amplified magnetic field. Neither interpretation can be excluded a priori. However, on the basis of sample data and a knowledge of likely anomaly sources on the lunar nearside, it is suggested here that basin ejecta are the most probable anomaly sources. In some cases these sources are probably buried beneath later mare basalt flows such as that within the Ingenii basin.

The strongest individual anomalies in both the Imbrium and Crisium antipode zones correlate (within observational error) with swirl-like albedo markings of the Reiner Gamma class (Plates 2 and 3). Swirls are most easily recognized when superposed on darker mare units but are also visible at the Crisium antipode in a highlands region. The concentration of magnetic anomalies and swirls in basin antipode zones (including also the Orientale and Serenitatis zones, not considered here) does not favor the cometary impact model for swirl origins. The Lunar Prospector data are therefore most consistent with the solar wind deflection model. Further tests of this model are possible using electron reflectometer data from low-altitude passes over the strongest anomalies. However, a final verification of the ion deflection model will probably require in situ measurements of both magnetic fields and energetic particle fluxes as a function of position at the lunar surface in regions where swirls are found.

Acknowledgments. Processing and mapping of the Lunar Prospector magnetometer data are supported by the NASA Lunar Data Analysis Program through a contract from the Lunar Research Institute. We thank C. Russell for a helpful critical review.

References

Anderson, K. A., and D. E. Wilhelms, Correlation of lunar farside magnetized regions with ringed impact basins, *Earth Planet. Sci. Lett.*, *46*, 107-112, 1979.

Anderson, K. A., R. Lin, R. McGuire, J. McCoy, C. Russell, and P. Coleman Jr., Linear magnetization feature associated with Rima Sirsalis, *Earth Planet. Sci. Lett.*, *34*, 141-151, 1977.

Bell, J., and B. R. Hawke, The Reiner Gamma Formation: Composition and origin as derived from remote sensing observations, *Proc. Lunar Planet. Sci. Conf. 12th*, 679-694, 1981.

Binder, A. B., W. C. Feldman, G. S. Hubbard, A. S. Konopliv, R. P. Lin, M. H. Acuna, and L. L. Hood, Lunar Prospector searches for polar ice, a metallic core, gas release events, and the Moon's origin, *EOS. Trans. AGU*, *79*, 97, 108-109, 1998.

Cisowski, S. M., D. W. Collinson, S. K. Runcorn, A. Stephenson, and M. Fuller, A review of lunar paleointensity data and implications for the origin of lunar paleomagnetism, *Proc. Lunar Planet. Sci. Conf. 13th*, Part 2, *J. Geophys. Res.*, *88*, suppl., A691–A704, 1983.

Fuller, M., Lunar magnetism, *Rev. Geophys.*, *12*, 23-70, 1974.

Fuller, M., and S. Cisowski, Lunar paleomagnetism, in *Geomagnetism*, vol. 2, edited by J. Jacobs, Ed., pp. 307–456, Academic, San Diego, Calif., 1987.

Gold, T., and S. Soter, Cometary impact and the magnetization of the Moon, *Planet. Space Sci.*, *24*, 45-54, 1976.

Halekas, J., D. Mitchell, R. Lin, S. Frey, M. Acuña, L. Hood, and A. Binder, Strong magnetic anomalies on the lunar near side, *Lunar Planet. Sci., XXXI*, 2000a.

Halekas, J., D. Mitchell, R. Lin, S. Frey, M. Acuña, L. Hood, and A. Binder, Mapping of the lunar crustal magnetic field by Lunar Prospector, *Lunar Planet. Sci., XXXI*, 2000b.

Haskin, L. A., The Imbrium impact event and the thorium distribution at the lunar highlands surface, *J. Geophys. Res.*, *103*, 1679–1689, 1998.

Hide, R., Comments on the Moon's magnetism, *Moon*, *4*, 39, 1972.

Hood, L., Bulk magnetization properties of the Fra Mauro and Reiner Gamma Formations, *Proc. Lunar Planet. Sci. Conf. 11th*, 1879-1896, 1980.

Hood, L., Sources of lunar magnetic anomalies and their bulk directions of magnetization: Additional evidence from Apollo orbital data, *Proc. Lunar Planet. Sci. Conf. 12th*, 817-830, 1981.

Hood, L., Magnetic field and remanent magnetization effects of basin-forming impacts on the Moon, *Geophys. Res. Lett., 14*, 844-847, 1987.

Hood, L., Frozen fields, *Earth Moon Planets, 67*, 131-142, 1995.

Hood, L., and Z. Huang, Formation of magnetic anomalies antipodal to lunar impact basins: Two-dimensional model calculations, *J. Geophys. Res., 96*, 9837-9846, 1991.

Hood, L., and G. Schubert, Lunar magnetic anomalies and surface optical properties, *Science, 208*, 49–51, 1980.

Hood, L., and A. Vickery, Magnetic field amplification and generation in hypervelocity meteoroid impacts with application to lunar paleomagnetism, *Proc. Lunar Planet. Sci. Conf. 15th*, Part 1, *J. Geophys. Res., 89*, suppl., C211-C223, 1984.

Hood, L., and C. Williams, The lunar swirls: Distribution and possible origins, *Proc. Lunar Planet. Sci. Conf. 19th*, 99–113, 1989.

Hood, L., P. J. Coleman Jr., and D. E. Wilhelms, The Moon: Sources of the crustal magnetic anomalies, *Science, 204*, 53-57, 1979a.

Hood, L., P. J. Coleman Jr., and D. E. Wilhelms, Lunar nearside magnetic anomalies, *Proc. Lunar Planet. Sci. Conf. 10th*, 2235-2257, 1979b.

Hood, L., C. T. Russell, and P. J. Coleman Jr., Contour maps of lunar remanent magnetic fields, *J. Geophys. Res., 86*, 1055-1069, 1981.

Housley, R. M., Solar wind and micrometeorite effects in the lunar regolith, *Philos. Trans. R. Soc. London, Ser. A, 285*, 363–370, 1977.

Keller, L. P., S. J. Wentworth, D. S. McKay, L. A. Taylor, C. Pieters, and R. V. Morris, Space weathering in the fine size fractions of lunar soils: Soil maturity effects, in *Workshop on New Views of the Moon II*, Lunar and Planet. Inst., Houston, Tex., 32–34, 1999.

Korotev, R., Compositional variation in Apollo 16 impact-melt breccias and inferences for the geology and bombardment history of the Central Highlands of the Moon, *Geochim. Cosmochim. Acta, 58*, 3931-3969, 1994.

Lawrence, D. J., D. L. Mitchell, A. Binder, R. Elphic, W. Feldman, S. Frey, J. Halekas, L. Hood, R. Lin, and S. Maurice, A comparison of Lunar Prospector thorium and magnetic field data within South Pole Aitken basin, *Lunar Planet. Sci., XXXI*, 2000..

Lin, R. P., K. A. Anderson, and L. Hood, Lunar surface magnetic field concentrations antipodal to young large impact basins, *Icarus, 74*, 529–541, 1988.

Lin, R. P., D. Mitchell, D. Curtis, K. Anderson, C. Carlson, J. McFadden, M. Acuña, L. Hood, and A. Binder, Lunar surface magnetic fields and their interaction with the solar wind: Results from Lunar Prospector, *Science, 281*, 1480–1484, 1998.

Lucey, P. G., G. J. Taylor, and B. R. Hawke, Global imaging of maturity: Results from Clementine and lunar sample studies, *Lunar Planet. Sci. XXIX*, 1998.

McCauley, J., Geologic map of the Grimaldi Quadrangle of the Moon, *U.S. Geol. Surv., Map I-740*, 1973.

Moore, H. J., C. Hodges, and D. Scott, Multi-ringed basins – Illustrated by Orientale and associated features, *Proc. Lunar Sci. Conf. 5th*, 71–100, 1974.

Pieters, C., E. Fischer, O. Rode, and A. Basu, Optical effects of space weathering: The role of the finest fraction, *J. Geophys. Res., 98*, 20,817–20,824, 1993.

Russell, C. T., P. J. Coleman Jr., B. K. Fleming, L. Hilburn, G. Ioannidis, B. R. Lichtenstein, and G. Schubert, The fine scale lunar magnetic field, *Proc. Lunar Sci. Conf. 6th*, 2955-2969, 1975.

Schultz, P., and D. Gault, Seismic effects from major basin formations on the Moon and Mercury, *Moon, 12*, 159–177, 1975.

Schultz, P., and L. J. Srnka, Cometary collisions on the Moon and Mercury, *Nature, 284*, 22–26, 1980.

Srnka, L. J., J. L. Hoyt, J. V. S. Harvey, and J. E. McCoy, A study of the Rima Sirsalis magnetic anomaly, *Phys. Earth Planet. Inter., 20*, 281-290, 1979.

Strangway, D. W., H. Sharpe, W. Gose, and G. Pearce, Lunar magnetic anomalies and the Cayley Formation, *Nature, 246*, 112–114, 1973a.

Strangway, D. W., W. Gose, G. Pearce, and R. McConnell, Magnetism and the history of the Moon, in *Magnetism and Magnetic Materials – 1972*, edited by C. Graham Jr. and J. Rhyne, pp. 1178–1187, Am. Inst. of Phys., New York, 1973b.

Stuart-Alexander, D. E., Geologic map of the central far side of the Moon, *U.S. Geol. Surv. Misc. Geol. Invest. Map, I-1047*, 1978.

Wentworth, S. J., L. P. Keller, D. S. McKay, and R. V. Morris, Space weathering on the Moon: Patina on Apollo 17 samples 75075 and 76015, *Meteorit. Planet. Sci., 34*, 593-603, 1999.

Wilhelms, D. E., and F. El-Baz, Geologic map of the east side of the Moon, *U.S. Geol. Surv. Misc. Geol. Invest. Map, I-948*, 1977.

M.H. Acuña, Goddard Space Flight Center, Greenbelt, MD 20771.

A.B. Binder, Lunar Research Institute, Tucson, AZ 85747.

J. Halekas, R.P. Lin, and D.L. Mitchell, Space Sciences Laboratory, University of California, Berkeley, CA 94729.

L.L. Hood, Lunar and Planetary Laboratory, University of Arizona, Kuiper Space Sciences Building, 1629 E. University Boulevard, Tucson, AZ 85721-0092. (lon@lpl.arizona.edu)

A. Zakharian, Center for Mathematical Sciences, University of Arizona, Tucson, AZ 85721.

(Received August 24, 2000; revised February 21, 2001; accepted March 13, 2001.)